Cell Reports
Article

Crystal Structure of Prp5p Reveals Interdomain Interactions that Impact Spliceosome Assembly

Zhi-Min Zhang,[1,3] Fei Yang,[2,3] Jinru Zhang,[1] Qing Tang,[2] Jie Li,[1] Jing Gu,[2] Jiahai Zhou,[1,*] and Yong-Zhen Xu[2,*]
[1]State Key Laboratory of Bio-organic and Natural Products Chemistry, Shanghai Institute of Organic Chemistry, Chinese Academy of Sciences, Shanghai 200032, China
[2]Key Laboratory of Insect Developmental and Evolutionary Biology, Institute of Plant Physiology and Ecology, Shanghai Institutes for Biological Sciences, Chinese Academy of Sciences, Shanghai 200032, China
[3]These authors contributed equally to this work
*Correspondence: jiahai@mail.sioc.ac.cn (J.Z.), yzxu@sibs.ac.cn (Y.-Z.X.)
http://dx.doi.org/10.1016/j.celrep.2013.10.047

SUMMARY

The DEAD-box adenosine triphosphatase (ATPase) Prp5p facilitates U2 small nuclear ribonucleoprotein particle (snRNP) binding to the intron branch site region during spliceosome assembly. We present crystal structures of *S. cerevisiae* Prp5p alone and in complex with ADP at 2.12 Å and 1.95 Å resolution. The three-dimensional packing of Prp5p subdomains differs strikingly from that so far observed in other DEAD-box proteins: two RecA-like subdomains adopt an "open state" conformation stabilized by extensive interactions involving sequences that flank the two subdomains. This conformation is distinct from that required for ATP hydrolysis. Consistent with this, Prp5p mutations that destabilize interdomain interactions exhibited increased ATPase activity in vitro and inhibited splicing of suboptimal branch site substrates in vivo, whereas restoration of interdomain interactions reversed these effects. We conclude that the Prp5p open state conformation is biologically relevant and that disruption of the interdomain interaction facilitates a large-scale conformational change of Prp5p during U2 snRNP-branch site recognition.

INTRODUCTION

Pre-mRNA splicing is catalyzed by the spliceosome, a highly dynamic massive ribonucleoprotein machine with five (U1, U2, U4, U5, and U6) small nuclear ribonucleoprotein particles (snRNPs) and dozens of non-snRNP factors (Will and Lührmann, 2011). Spliceosome assembly is a stepwise process that forms networks of RNA-RNA and RNA-protein interactions (Warf and Berglund, 2010). Eight spliceosomal DExD/H proteins (also referred to as adenosine triphosphatases [ATPases]/RNA helicases), including Sub2p, Prp5p, Prp28p, Brr2p, Prp2p, Prp16p, Prp22p, and Prp43p, are essential for pre-mRNA splicing (Staley and Guthrie, 1998). It has been proposed that DExD/H proteins function as motors to rearrange structures by unwinding RNA duplexes and participate in all aspects of RNA metabolism, including transcription, pre-mRNA splicing, RNA transport and decay, ribosome biogenesis, translation, and micro-RNA processing (Bleichert and Baserga, 2007; Jankowsky and Fairman, 2007; Linder and Jankowsky, 2011). Using energy from cycles of ATP binding and hydrolysis, these ATPases are assumed to rearrange structures during spliceosome assembly and disassembly by either unwinding short RNA-RNA duplexes or removing RNA-interacting proteins (Linder, 2006; Staley and Guthrie, 1998). For example, facilitated by Prp28p, the early 5′SS-U1 small nuclear RNA (snRNA) interaction is exchanged for a 5′SS-U6 snRNA interaction prior to formation of spliceosomal complex B (Staley and Guthrie, 1999; Strauss and Guthrie, 1994). Likewise, facilitated by Brr2p, the U4–U6 snRNA interaction in the U4/U6-U5 tri-snRNP is replaced by U2–U6 snRNA interaction during formation of the "activated spliceosome" (Maeder et al., 2009; Mozaffari-Jovin et al., 2012). In addition, the target of Brr2p (Hahn et al., 2012) and structures of Brr2p in complex with subdomains of Prp8p (Mozaffari-Jovin et al., 2013; Nguyen et al., 2013) have been recently revealed, providing an example of functional studies of spliceosomal ATPase by genetics and structural biology.

DEAD-box proteins, termed by their signature motif II (Asp-Glu-Ala-Asp; D-E-A-D), are the largest subfamily of DExD/H proteins. Three DEAD-box proteins are involved in pre-mRNA splicing: Sub2p/UAP56, Prp5p, and Prp28p. All DEAD-box proteins contain a highly conserved ATPase/helicase core domain that comprises two RecA-like subdomains (denoted D1 and D2) and are characterized by 11 motifs, including motifs Q, I, Ia, GG, Ib, II, and III in D1 and motifs IV, QxxR, V, and VI in D2 (Jankowsky and Fairman, 2007). Additional N- and C-terminal sequences flanking the core domain are usually present to provide auxiliary functional specificities (Banroques et al., 2011). Crystal structures of the core ATPase/helicase domains from several DEAD-box proteins, such as eIF4A, Vasa, Mss116p, mjDEAD, and spliceosomal ATPase UAP56, have been determined (Bono et al., 2006; Caruthers et al., 2000; Del Campo

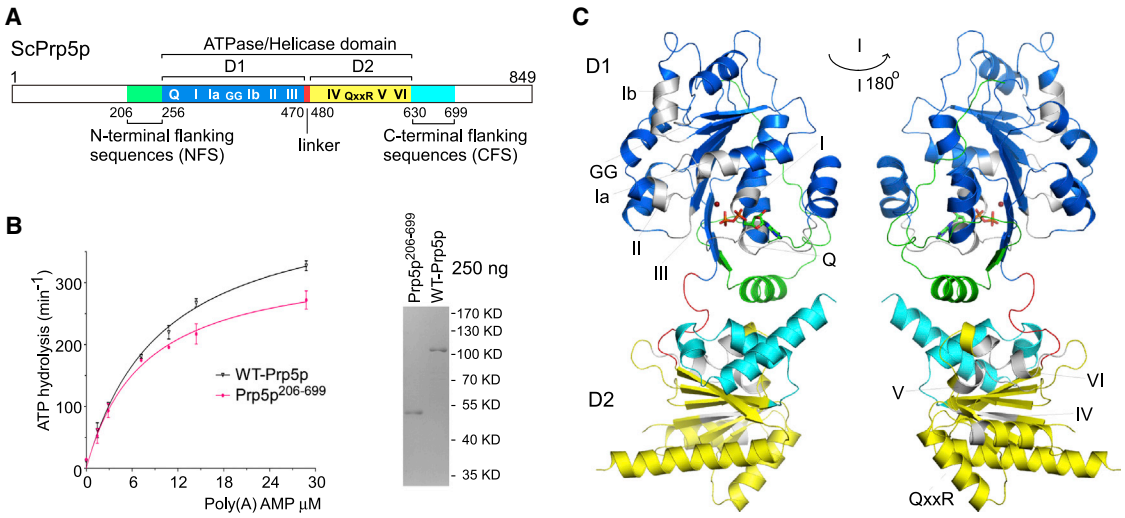

Figure 1. A Twisted Open State Structure of Prp5p

(A) Schematic of S. *cerevisiae* Prp5p protein. The highlighted region (aa 206–699) was used for crystallization. Green, NFS; blue, D1; yellow, D2; red, subdomain linker; cyan, CFS. Colors are used similarly in other places unless otherwise indicated.

(B) $Prp5p^{206–699}$ for crystallization is active to hydrolyze ATP. (Left) In vitro ATPase activities of full-length Prp5p and $Prp5p^{206–699}$. Concentration of AMP is used due to the heterogeneous length of poly(A). Curves are drawn by GraphPad Prism 5. The error bars indicate the SD from the mean value obtained from at least two experiments. (Right) Purified proteins (250 ng for each) were separated by SDS-PAGE and visualized by Coomassie blue staining.

(C) Overall structure of the Prp5p-Mg^{2+}ADP complex. The final model of this structure is at the resolution of 1.95 Å and contains residues 211–512 and 525–673. Conserved motifs (gray) in D1 and D2 domains are on opposite surfaces of Prp5p protein. Mg^{2+} (red sphere) and ADP (sticks) are indicated.

and Lambowitz, 2009; Mallam et al., 2012; Sengoku et al., 2006; Shi et al., 2004; Story et al., 2001) and revealed that there are conformational changes of D1 and D2 from a flexible "open state" to a compact "closed state" upon RNA binding (Bono et al., 2006; Del Campo and Lambowitz, 2009; Sengoku et al., 2006). However, detected by small-angle X-ray scattering, a solution structure of full-length Mss116p in the absence of RNA substrate was found in a stable open state conformation with D1 and D2 in a preferred relative orientation, suggesting that additional flanking sequences might affect the overall structures of the core helicase domains (Mallam et al., 2011).

Prp5p, one of the spliceosomal DEAD-box proteins, is involved in the early stage of spliceosome assembly (Dalbadie-McFarland and Abelson, 1990; Ruby et al., 1993) and genetically interacts with numerous proteins and RNA components of U2 snRNP (Perriman and Ares, 2000; Ruby et al., 1993; Wells and Ares, 1994; Wells et al., 1996; Yan and Ares, 1996). Like other DEAD-box proteins, the D1 and D2 subdomains of Prp5p are connected by a short linker and characterized by 11 conserved motifs. The ATPase activity of Prp5p is required for the formation of prespliceosome (U1/U2/pre-mRNA) complexes, and distinct domains in the N terminus of Prp5p were identified to separately interact with U1 and U2 snRNPs (Shao et al., 2012; Xu et al., 2004). Deletion of Cus2, a component of U2 snRNP, allows U2-intron branch-site region (BS) binding in the absence of ATP, although Prp5p is still physically required (Perriman and Ares, 2000; Perriman et al., 2003), suggesting that one result of Prp5p activity is removal of Cus2p and its target might be an internal structure of U2 snRNA (Perriman and Ares, 2010). Prp5p also modulates splicing fidelity through competition with the stability of BS:U2 snRNA duplex at the stage of prespliceosome assembly (Xu and Query, 2007). However, function and structure of ATPase Prp5p demand further research.

To understand the molecular mechanism of Prp5p function, we determined crystal structures of *S. cerevisiae* Prp5p alone (2.12 Å) and in complex with Mg^{2+}-ADP (1.95 Å). These structures reveal an open state conformation, in which the D1 and D2 subdomains are stabilized by extensive interdomain interactions of residues from the subdomain linker with both N- and C-terminal flanking segments. In vitro assays show that mutant Prp5p proteins with destabilized interdomain interactions have faster-than-wild-type (WT) activation of Prp5p to form Prp5p-ATP-RNA intermediate and result in increased ATPase activities. Furthermore, such mutant *prp5* alleles in budding yeast specifically inhibit splicing of suboptimal BS substrates, demonstrating that this twisted open state conformation of Prp5p is biologically relevant to spliceosome assembly at the time of U2 snRNP addition to the intron branch site.

RESULTS

Overall Structures of Prp5p and Its Complex with ADP

After extensive trials, we identified a fragment of *S. cerevisiae* Prp5p ($Prp5p^{206–699}$) containing the conserved ATPase/helicase core domain (D1: amino acid [aa] 256–470; D2: aa 480–629), an additional N-terminal flanking sequence (NFS; aa 206–255), and a C-terminal flanking sequence (CFS; aa 630–699) that was soluble, highly expressed in bacteria, and whose ATPase activity in vitro was similar to that of the full-length Prp5p (Figures 1A and 1B). We succeeded in obtaining crystals and solving structures of $Prp5p^{206–699}$ with and without Mg^{2+}-ATP present in the crystallization solution (Table 1; Figure S1A). In the presence of

Table 1. Data Collection and Refinement Statistics

	Prp5p-Mg^{2+}ADP (PDB ID: 4LJY)	Apo-Prp5p (PDB ID: 4LK2)	Apo-Prp5p[a]
Data Collection			
Space group	$P4_32_12$	$P2_12_12_1$	$P4_12_12$
Cell Dimensions			
a, *b*, *c* (Å)	90, 90, 90	90, 90, 90	90, 90, 90
α, β, γ (°)	85.3, 85.3, 124.9	87.2, 86.1, 128.0	87.0, 87.0, 383.6
Wavelength	0.9792	0.9792	0.9792
No. of protein in per asu[b]	1	2	3
Resolution (Å)	43.3–1.90 (1.97–1.90)[c]	38.88–2.05 (2.12–2.05)	47.99–2.56 (2.65–2.56)
R_{sym} or R_{merge}	0.105 (0.876)	0.112 (0.793)	0.166 (0.8)
$I/\sigma I$	25.3 (3.5)	12.3 (2.5)	21.36 (2.9)
Completeness (%)	98.5 (95.0)	97.28 (96.89)	97.00 (100.0)
Redundancy	17.8	4.6	9.3
Refinement			
Resolution (Å)	1.95	2.12	2.60
No. reflections	34,921	51,501	43,808
R_{work}/R_{free}	0.20/0.23	0.21/0.25	0.23/0.29
No. atoms			
Protein	3,550	6,775	
Ligand/ion	44	1	
Water	255	237	
B-factors			
Protein	35.80	43.20	
Ligand/ion	33.60	32.95	
Water	38.30	40.00	
Rmsd			
Bond lengths (Å)	0.007	0.008	
Bond angles (°)	1.139	1.086	

[a]Refinement was not completed because the overall structure from this data set was almost identical to that from the data at 2.05 Å resolution.
[b]asu, asymmetric unit.
[c]Values in parentheses are for highest-resolution shell. Each data set was collected from a single crystal.

ATP and Mg^{2+}, the obtained crystals belong to space group $P4_32_12$, and the complex structure was determined by single anomalous diffraction (SAD) and refined to 1.95 Å resolution (Figures 1C and S1B). The final model contains residues 211–512 and 525–673. The electron density for ADP became unambiguous after refinement, whereas the density for the γ-phosphate of ATP was not detected, indicating that ATP had been hydrolyzed during crystallization. This complex is referred to hereafter as Prp5p-Mg^{2+}ADP. The structure of Prp5p alone (apo-Prp5p) was solved by molecular replacement and refined to 2.12 Å. The crystals of apo-Prp5p belong to space group $P2_12_12_1$ and contain two molecules (referred to as chains A and B) per asymmetric unit. Both chains can be superimposed with the Prp5p-Mg^{2+}ADP structure within root-mean-square deviations (rmsds) of 1.4–1.7 Å over all the Cα atoms (Table 1; Figure S1A), suggesting that few conformational changes occurred to Prp5p upon ATP/ADP binding.

The overall structure of Prp5p is organized into a dumbbell shape with D1 and D2 flanked by residues from the NFS and CFS (Figure 1C). D1 comprises a seven-stranded parallel β sheet surrounded by eight helices and interacts with an antiparallel β strand (β1) in the NFS. D2 contains a six-stranded central parallel β sheet packed against five helices and interacts with helix α2 in the NFS and helix α17 in the CFS (Figures S2).

An Unusual Twisted Conformation of Prp5p

The secondary and tertiary structures of D1 and D2 in Prp5p are well conserved with other DEAD-box proteins when separately aligned with their counterparts in UAP56, Mss116, and Vasa (Figures S2B and S3). However, in Prp5p, the three-dimensional packing of D1 and D2 (Figure 1C) is strikingly different from that so far observed in other DEAD-box proteins, such as mjDEAD and UAP56 (Shi et al., 2004; Story et al., 2001). The Prp5p structure adopts an open state conformation, twisted relative to the other structures, by placing the highly conserved helicase motifs in D1 and D2 (found clustered together in other DEAD-box protein structures) on opposite sides of the Prp5p structure. Motifs in D1 involved in ATP binding (Q, I, and II) and ATP hydrolysis (III), as well as motifs Ia, GG, and Ib, are located on one surface of Prp5p (Figure 1C, left), whereas motifs IV, QxxR, V, and VI from D2, potentially responsible for RNA-binding or ATP coordination, are found on the opposite surface (Figure 1C, right). In addition, the NFS inserts into a groove between D1 and D2 and wraps around D1 close to the outmost strand of the central β sheet; the CFS folds into a single turn of a right-handed super-helix formed by helices 17–19 (Figures 1C and S2A).

ATP-Binding Sites

As has been observed in other DEAD-box proteins (Caruthers et al., 2000; Del Campo and Lambowitz, 2009; Mallam et al., 2012; Sengoku et al., 2006; Shi et al., 2004; Story et al., 2001; Tanner and Linder, 2001), conserved residues from motifs Q, I, and II in D1 of Prp5p interact with the ribose moiety, α and β phosphates of ADP, and a magnesium ion (Figure 2A). The adenine ring of ADP is stacked against F276 and forms hydrogen bonds with Q283 via N6 and N7 and with the side chain of S278 via N6. Additionally, the main chains of G277 and S278 interact with N1 through a water molecule. In motif Q, Q283 is the most conserved and the signature residue, exhibiting conserved contacts with ADP as observed in other DEAD-box proteins (Högbom et al., 2007; Shi et al., 2004). Although residues F276, G277, and S278 in Prp5p are not conserved in other DEAD-box proteins, they provide similar interactions with the adenine ring as do residues adjacent to the signature glutamine in DDX3X (Högbom et al., 2007). The α and β phosphates of ADP are held by main chain atoms of residues from 304 to 308 ($_{304}$SGKTI) in Prp5p with extensive hydrogen bonds, in which G305, K306, and T307 are the most conserved residues in motif I of DEAD-box proteins. A magnesium ion is clearly distinguishable in the structure, which coordinates in an octahedral geometry to an oxygen atom of the β-phosphate of ADP and to five water molecules, two of which are hydrogen-bonded with

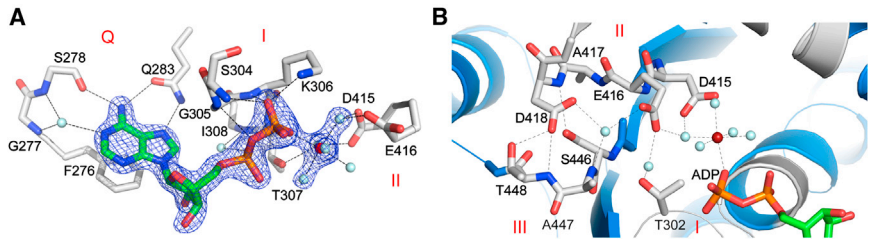

Figure 2. ATP-Binding Sites of Prp5p

(A) Residues from motifs Q (F276, G277, S278, Q283), I (S304–I308), and II (D415 and E416) of Prp5p interact with the adenine ring and α- (green) and β (orange) -phosphates of ADP molecule. The Mg^{2+} (red sphere) is coordinated to an oxygen atom of β-phosphate and five waters (white spheres).

(B) Residues in motif III strongly interact with motif II through multiple hydrogen bonds, suggesting that motif III is also involved in the ATPase activity of Prp5p.

the side chains of D415 and T307 (Figure 2A). Therefore, these contacts between conserved residues and ADP are similar to those observed in other DEAD-box proteins, such as DDX3X, UAP56, and eIF4A (Caruthers et al., 2000; Högbom et al., 2007; Shi et al., 2004). The major difference for ADP-binding between Prp5p and other DEAD-box proteins is that the ADP-binding site of Prp5p is located on the surface of D1 (Figure 1C), whereas the counterparts in mjDEAD and UAP56 are in the clefts formed between their D1 and D2 (Shi et al., 2004; Story et al., 2001).

Although residues in motif III (SAT_{448}) do not directly interact with ADP or Mg^{2+}, they have multiple interactions with residues in motif II. The carboxyl group of D418 in motif II forms two hydrogen bonds with S446 and T448 from motif III; the imino group of D418 also forms a hydrogen bond with S446. Moreover, E416 and D418 are pulled together with residue A447 from motif III through water molecules (Figure 2B). These extensive interactions between motifs II and III suggest that motif III is strongly linked with ATP binding and hydrolysis, consistent with previous findings of random mutation screenings in motif III of Prp5p. For example, *prp5*-SA$\underline{G}_{448}$ and $\underline{G}A\underline{G}_{448}$ alleles showed decreased ATP hydrolysis activities and altered splicing fidelity; *prp5*-$\underline{G}A\underline{R}_{448}$ and SA$\underline{W}_{448}$ alleles showed more seriously decreased ATP hydrolysis activities and even growth defects (Xu and Query, 2007). From the structure of Prp5p, it is clear that mutation of residue T448 in motif III to Gly abolishes its hydrogen-bond interaction with residue D418 in motif II; mutation of T448 to Arg or Trp might cause steric conflicts, thereby altering ATP hydrolysis and splicing activity.

The Twisted Conformation Is Stabilized by Extensive Interdomain Interactions

In the absence of an RNA substrate, contacts between D1 and D2 are typically rare in previously reported structures; for example, D1 and D2 of eIF4A exist in multiple relative orientations and move independently to each other via their flexible linkers in the absence of bound RNA (Caruthers et al., 2000). The two subdomains are pulled together after RNA substrate accommodation. In contrast, we propose that the twisted conformation of Prp5p is rigid in the absence of RNA substrate and the D1 and D2 subdomains cannot move independently of each other (Figure 3A).

In support of this, first the subdomain linker between D1 and D2 of Prp5p is stabilized by multiple hydrogen-bond interactions between residues in the NFS, CFS, and water molecules to adopt a fixed, no-longer-free-to-move conformation (Figure 3B). For example, the carbonyl group of the linker residue K472 interacts directly with the Nδ2 atom of N242 in the NFS; linker residues N470, S471, G473, and M474 form four water-mediated hydrogen bonds with residue N242; and residue N476 in the subdomain interacts with V610 and G614 in D2 through water molecules. The nearby residues V475 and N476 provide a network of hydrogen-bond interactions with Q481 in D2 and with A643 and E648 in CFS via their amide or carbonyl groups. Second, a hydrophobic region dominates the interdomain surface. Residues around the hydrophobic region include L238 from NFS; M474 and V475 from the subdomain linker; F606, Y609, and V610 from D2; and I639, L640, A643, and M644 from a right-handed superhelix in CFS (Figure 3C). Moreover, residue E235 in the NFS strongly interacts with the amide groups of F606 and A607 from D2 through two hydrogen bonds.

Taken together, these contacts argue that the twisted conformation of Prp5p is maintained by extensive interdomain interactions between subdomains, the subdomain linker, and two flanking sequences.

Destabilization of the Twisted Conformation Results in Faster Activation of Prp5p

If the twisted open state conformation of Prp5p is biologically relevant and its disruption is required to form a closed and active conformation, then we predicted that mutations that destabilize the twisted Prp5p form might have observable effects on its ATPase activity and function at the early stage of spliceosome assembly. To test this hypothesis, we mutated a number of key residues involved in the interdomain interactions and compared the ATPase activities of WT and mutant Prp5p recombinant proteins. The ATPase activity by Prp5p could be divided into two steps: binding of ATP and RNA (formation of Prp5p-ATP-RNA) and hydrolysis of ATP (formation of Prp5p-ADP-RNA). The measured $K_{m(RNA)}$ represents the ability of Prp5p to associate with RNA substrate, and k_{cat} represents the rate of ATP hydrolysis by Prp5p (Figure 4A). In comparison to WT Prp5p, the previously identified motif III mutant protein Prp5p-SA$\underline{G}$ (Xu and Query, 2007) exhibited a lower ATPase activity and a decreased k_{cat}, indicating that mutant Prp5p-SA$\underline{G}$ protein is defective in hydrolyzing ATP (Figure 4A). In contrast, mutant protein Prp5p-E235A (that would abolish the two hydrogen-bond interactions with residues F606 and A607) and mutant proteins Prp5p-L238A and -F606A (that would impair the hydrophobic interactions at the interdomain surface) exhibit higher ATPase activities with similar k_{cat} but significant lower $K_{m(RNA)}$, indicating that their improved ATPase activity is due to faster activation to form Prp5p-ATP-RNA intermediate (Figure 4A). Consistent with these effects being specifically due to reduced

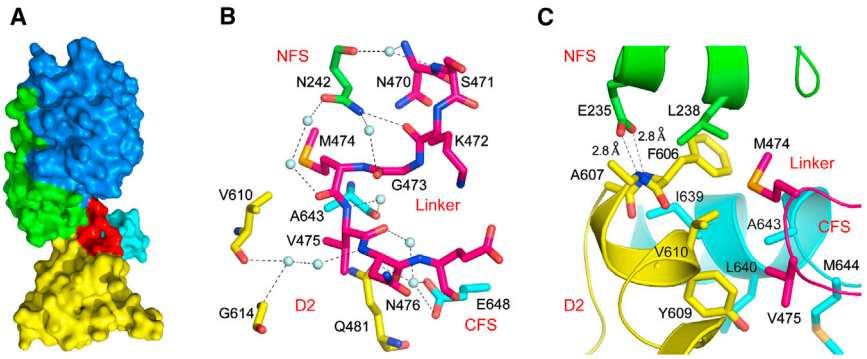

Figure 3. The Twisted Conformation of Prp5p Is Stabilized by Extensive Interdomain Interactions that Involve Both N- and C-Terminal Flanking Sequences and the Subdomain Linker

(A) Surface representation of the Prp5p structure.

(B) Interaction network around the linker region. The subdomain linker is stabilized by multiple hydrogen bond interactions between residues from NFS, CFS, and D2.

(C) A hydrophobic region dominates the interdomain surface, which contains residues from D2, NFS, CFS, and the subdomain linker.

Hydrogen bonds and residues that contribute to the interdomain interactions are indicated. Same colors are used as Figure 1.

stability of the twisted structure, the double-mutation-containing Prp5p-F606A&I639F, in which the additional I639F mutation is predicted to restore the hydrophobic interaction disrupted by F606A mutation, has k_{cat} and $K_{m(RNA)}$ values similar to WT-Prp5p. We conclude that the mutant Prp5p proteins with destabilized conformations have a faster activation and result in increased ATPase activity.

In addition, it was reported that a *prp5* allele containing only the N-terminal half (1–492 aa), in which D2 and the entire C-terminal segment of Prp5p were deleted, is viable in the absence of Cus2 and presence of U2 snRNA branch-point interaction stem-loop (BSL) mutants (Perriman and Ares, 2010). Therefore, we asked whether the C-terminal segment (aa 700–849) would affect the ATPase activity and viability of the above Prp5p site-directed mutants. Deletion of the C-terminal segment slightly decreased the ATPase activity of Prp5p (less than 15%); however, this subtle effect was also observed in the Prp5p-E235A mutant protein (Figure S4B). Furthermore, in vivo analysis of deletion of the N-terminal (aa 1–205) and/or C-terminal segments (aa 700–849) resulted in lethality in *S. cerevisiae* (Figure S4C). This result suggests that the C-terminal segment did not obviously affect the ATPase activity of Prp5p but is important for Prp5p function.

Destabilization of the Twisted Conformation of Prp5p Specifically Inhibits Splicing of Suboptimal BS Substrates

To test whether this conformation of Prp5p is relevant during spliceosome function, we generated *prp5* alleles in *S. cerevisiae* carrying mutations that impair the interdomain interactions and destabilize the twisted conformation of Prp5p. The *ACT1-CUP1* reporter system was used to monitor splicing activities by conferring resistance to the presence of copper in the growth media (Figure 4B; Lesser and Guthrie, 1993; Xu and Query, 2007). In comparison to WT-*PRP5*, all the mutant *prp5* strains have no obvious growth defects (Figure S4A). However, mutant alleles *prp5*-E235D and -E235A that weaken or abolish the two hydrogen bonds with F606/A607 specifically inhibit splicing of the BS mutant reporters U257C, A258U, and A258C (each of which disrupts base pairs with U2 snRNA), but not of WT reporter or of 5′SS or 3′SS mutants (Figure 4C). The extent of inhibition of splicing by these two alleles is consistent with the extent to which each mutant would disrupt hydrogen-bond interaction that was observed in the crystal structure of Prp5p. Similarly, *prp5*-L238A and F606A alleles, which impair hydrophobic interactions at the interdomain surface, also specifically inhibit splicing of the BS region mutant reporters, but not of WT reporter or of 5′SS or 3′SS mutants (Figure 4D). Again, additional mutation of I639F together with *prp5*-F606A (*prp5*-F606A&I639F), which is predicted to restore the hydrophobic interaction, fully rescued splicing of BS mutant reporters that are inhibited by the F606A single mutation (Figure 4D). These results indicate that the twisted and stable conformation of Prp5p before RNA binding is biologically relevant to splicing proofreading and that disruption of this twisted conformation occurs at the time of U2 snRNP recognition of the intron branch site.

Fast and Slow *prp5* Alleles Reciprocally Suppress Each Other

The identified *prp5* alleles with altered ATPase activities and splicing activities of suboptimal BS mutant reporters can be classified into two categories: (a) slow alleles that enhance splicing of suboptimal BS substrates, isolated from previous genetic screens, and (b) fast alleles that inhibit splicing of suboptimal BS substrates, generated based on the Prp5p structures we obtained. Slow *prp5* alleles include mutants in motifs III (SAT) and DPLD[140], the latter having been characterized as a locus for interaction with the U2 snRNP heteroheptameric SF3b complex (Shao et al., 2012). All together, these *prp5* alleles represent altered Prp5p activities at various steps: mutants in the DPLD motif decrease the recruitment of Prp5p to early U2 snRNP; mutants that destabilized interdomain interactions increase the activation of Prp5p; and mutants in motif III decrease the ATP hydrolysis activity of Prp5p (Figure 5A). As described above, the six *prp5* alleles with single mutations either improve or inhibit splicing of suboptimal BS substrates U257C, A258C, and A258U, but none of them alters splicing of WT reporter (Figure 5B). Interestingly, all the combinations of one fast and one slow mutation in the same *prp5* allele provide reciprocal cancellation effects on splicing and restore splicing activities of suboptimal BS substrates to the levels close to that of WT-Prp5p (Figure 5B), demonstrating that disruption of the twisted and stable conformation of Prp5p resulted in an opposite splicing proofreading effect to the previous identified slow ATPase Prp5p mutants from genetic screens.

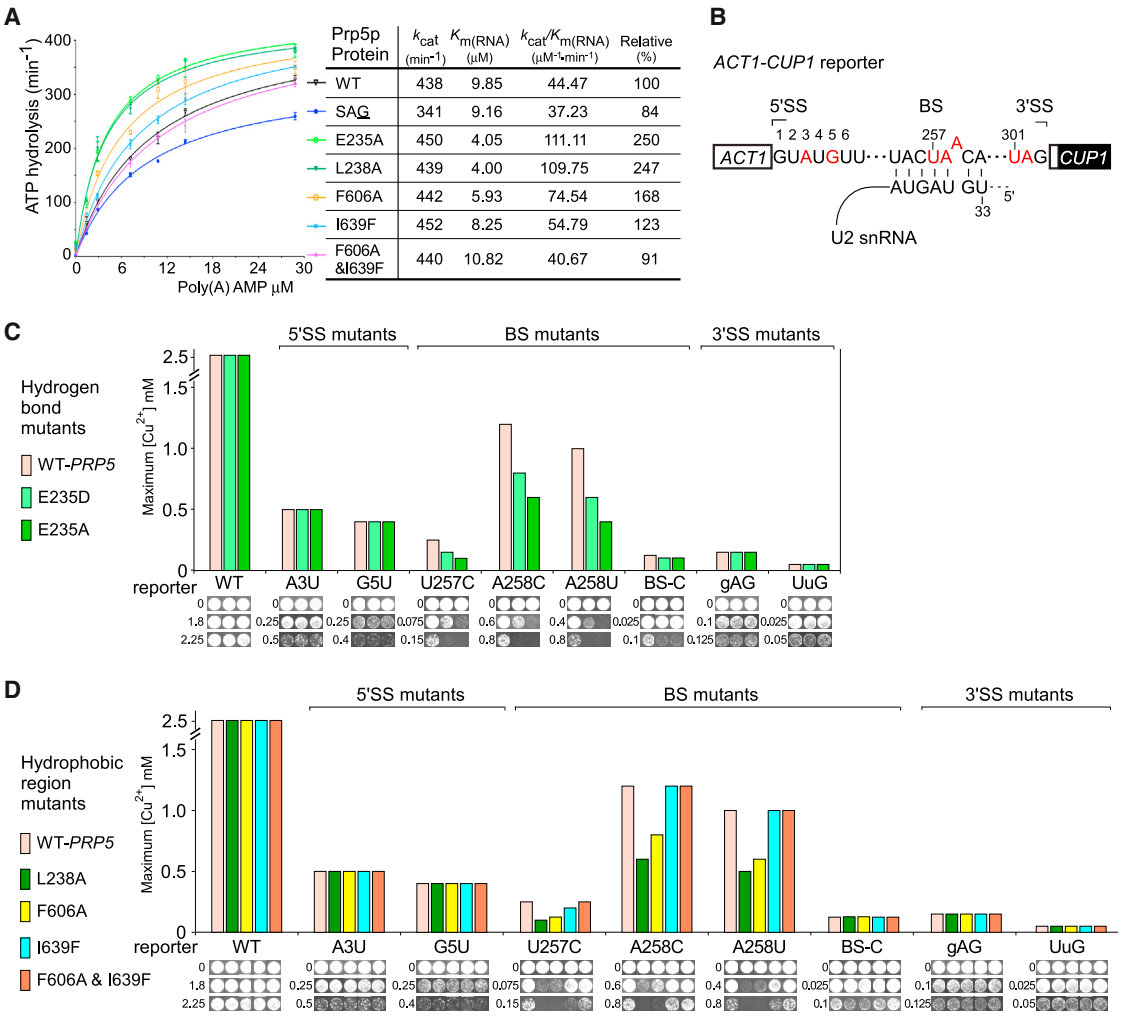

Figure 4. Destabilization of the Interdomain Interactions of Prp5p Increases Its ATPase Activity In Vitro and Specifically Enhances Splicing Fidelity at BS Region In Vivo

(A) ATPase assay of Prp5p proteins (left). Concentration of AMP is used due to the heterogeneous length of poly(A). Curves are drawn by GraphPad Prism 5. The error bars indicate the SD from the mean value obtained from at least two experiments. Improved ATPase activity of Prp5p mutants with less-stable interdomain interaction is due to faster activation to form Prp5p-ATP-RNA intermediates (right). k_{cat} and $K_{m(RNA)}$ were determined from data in the left.

(B) Schematics of *ACT-CUP1* pre-mRNA reporters used for monitoring splicing effects in vivo. Pairing region of U2 snRNA to the branch-site region is presented.

(C and D) *prp5* alleles that, with impaired hydrogen bonds formed by residue 235, and *prp5* alleles that, with weakened hydrophobic region, specifically inhibit splicing activity of suboptimal BS substrates. Splicing activities were determined by the maximum growth on copper medium. Copper concentrations shown were selected to illustrate the altered splicing activities.

DISCUSSION

The Open State Conformation of Prp5p Is Twisted and Stable

All of the Prp5p structures we obtained in this study adopted an elongated conformation in an open state, where the RecA-like D1 and D2 subdomains were well defined. Previously reported crystal structures of other DEAD-box proteins before RNA binding do not have such a rigid structural module, which might be due to a lack of sufficient N- and C-terminal flanking sequences. However, similar rigid conformations in the absence of RNA ligands were also observed in solution by small-angle X-ray scattering for two full-length DEAD-box proteins, Mss116p and CYT-19 (Mallam et al., 2011), indicating that, with additional flanking sequences or domains, the stable and rigid conformation before RNA substrate binding might be a feature common to DEAD-box proteins.

The distinct conformation of Prp5p is unlikely due to crystal packing, because the apo-Prp5p and its Mg^{2+}-ADP complex crystals we obtained belong to different space groups. Moreover, the 2.56 Å structure of another apo-Prp5p crystal (with space group $P4_12_12$ and three molecules per asymmetric unit) obtained under different growth condition is in a similar twisted conformation (Table 1). In addition, our further yeast mutagenesis studies of *prp5* alleles, which contain mutations to impair the interdomain interactions and destabilize the twisted

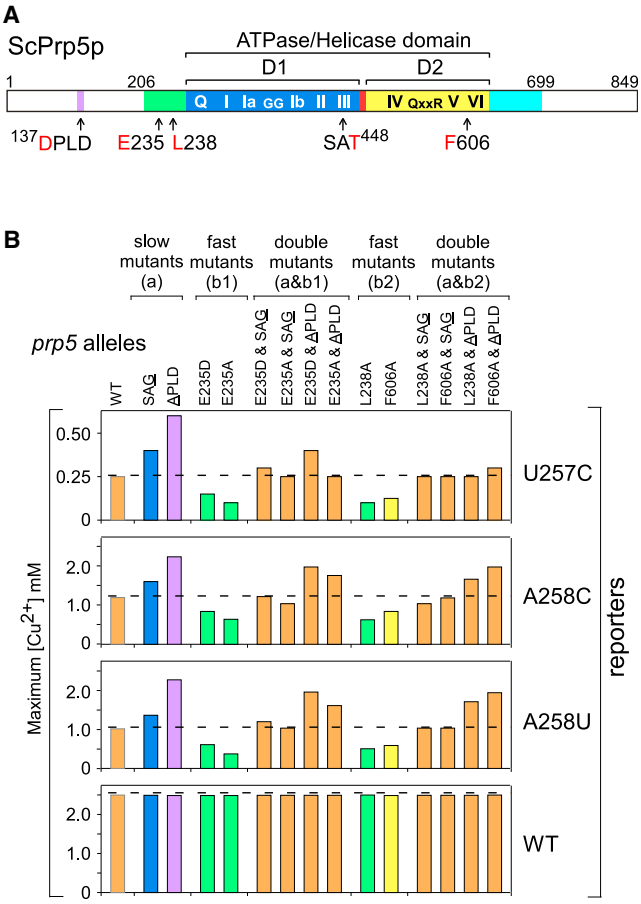

Figure 5. Slow and Fast *prp5* Mutant Alleles Mutually Rescue Each Splicing Defects

(A) Positions of mutated residues in the tested *prp5* alleles.

(B) Copper assays for splicing reporters in the presence of *prp5* alleles that contain either single or double mutations. Double-mutation *prp5* alleles, containing one from slow and one from fast alleles, mutually suppressed each splicing defect to the levels close to that of WT-PRP5.

conformation, specifically inhibit splicing of suboptimal BS substrates, and the double-mutation containing *prp5* allele with restored interdomain interactions rescues the splicing defects, providing strong evidence that this conformation of Prp5p indeed exists in vivo and is biologically relevant to pre-mRNA splicing activity.

A Large-Scale Conformational Change Is Required for Prp5p to be Active

Structural similarities between DEAD-box proteins revealed that the open state conformation, which is bound with ATP, must be remodeled to a closed state for efficient RNA-binding and ATP hydrolysis (Bono et al., 2006; Del Campo and Lambowitz, 2009; Mallam et al., 2012; Sengoku et al., 2006). When the D1 subdomain in the open state Prp5p we obtained is superimposed with the D1 in the closed state of Mss116p (Protein Data Bank [PDB] ID: 3I5X; Del Campo and Lambowitz, 2009), D2 of Prp5p requires a 182° rotation to match the D2 in the closed state of Mss116p to form a closed state Prp5p (Figure 6A). This suggests that a large-scale conformational change of Prp5p must occur for eventual RNA substrate accommodation, and the multiple interdomain interactions of Prp5p identified here must be disrupted to allow this conformational change. Prp5p mutants with a destabilized twisted conformation and higher ATPase activities would have a faster-than-WT transition from the open state to the closed state conformation. This large-scale conformational change might be triggered by interactions between Prp5p and other splicing factor(s) or specific RNA substrates during the formation of the prespliceosome. Previous studies found that *S. cerevisiae* Prp5p interacts with U2 snRNP component SF3b-155 by yeast two-hybrid assays (Wang et al., 2005), and *S. pombe* Prp5p interacts with SF3b subunits through its DPLD motif and with U1 snRNP through an serine/arginine-rich protein-like protein Rsd1 (Shao et al., 2012), which provided candidates for further investigations. An analogous example to the large-scale conformational changes of Prp5p in spliceosome assembly is that a "hydrophobic gate" in the structure of translation elongation factor (EF)-Tu with guanosine triphosphate (GTP) must be opened for catalytic residue His-84 to access the GTP-binding pocket and activate GTP hydrolysis; such conformational changes of EF-Tu are induced by the ribosome (Berchtold et al., 1993; Kjeldgaard et al., 1993; Villa et al., 2009).

The Stability of the Open State Conformation of Prp5p Affects Spliceosome Assembly and Splicing Fidelity

Most of the eight spliceosomal ATPases have been demonstrated to modulate splicing fidelity at various stages during spliceosome assembly and catalysis through characterization of mutant ATPases with defective ATP hydrolysis activities (Konarska et al., 2006; Koodathingal et al., 2010; Mayas et al., 2006; Semlow and Staley, 2012; Xu and Query, 2007; Yang et al., 2013). Isolated from a series of genetic screens, slow prp5 alleles improved splicing of suboptimal BS substrates and decreased splicing fidelity (Shao et al., 2012; Xu and Query, 2007). In this study based on the X-ray structural information, we designed and obtained fast prp5 alleles that specifically inhibit splicing of suboptimal BS substrates, linking the tertiary structure of ATPase with its modulation of splicing fidelity and demonstrating that the twisted open state conformation of Prp5p is critical for spliceosome assembly and splicing proofreading. It was proposed that a BSL structure in U2 snRNA forms prior to interaction with the intron and is disrupted by ATPase Prp5p during engagement of the snRNA with the intron (Perriman and Ares, 2010), and we previously found that there is a competition between the pairing of BS:U2 snRNA duplex and conformational changes facilitated by Prp5p (Xu and Query, 2007). Evidence from this study demonstrated that there is a large-scale conformational change of Prp5p from a twisted and stable open state to a closed state during the branch-site recognition in order to activate Prp5p ATPase and to commit the intron to the splicing pathway via stable U2 snRNP binding. For suboptimal BS substrates, the pairing of BS:U2 snRNA duplex is inefficient, mutant Prp5p, in which its interdomain interaction is destabilized and exhibits faster transition from the twisted open state to the closed state, would function faster to disrupt the BSL structure

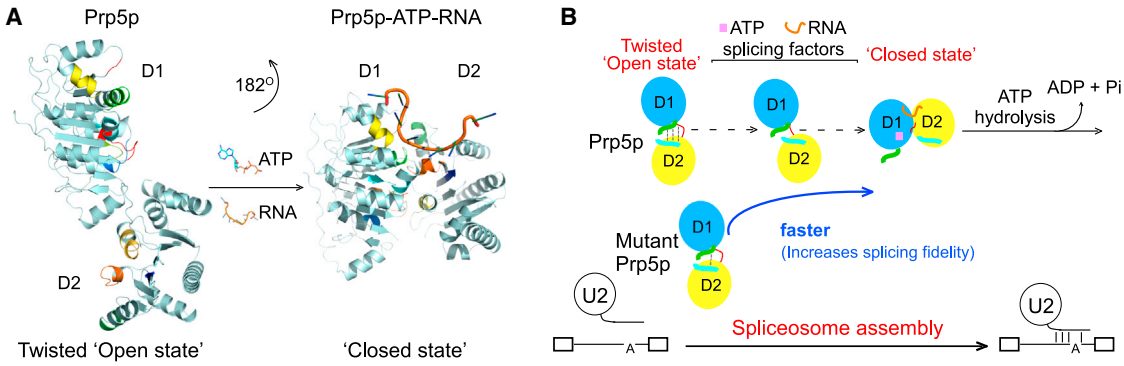

Figure 6. A Large-Scale Conformational Change of Prp5p from the Twisted Open State to the Closed State Is Required for Spliceosome Assembly

(A) Structural comparison of Prp5p with Mss116p-Mg^{2+}AMP-PNP-U_{10} (Del Campo and Lambowitz, 2009), indicating that the interdomain interactions in Prp5p must be disrupted for the large-scale conformational change from the twisted and stable open state to an active closed state.

(B) Conformational change of Prp5p is required for spliceosome assembly at the time of U2 snRNP addition to the intronic branch-site region. The twisted conformation of Prp5p is stabilized by extensive interdomain interactions (gray dashed) that involve NFS (green line), CFS (cyan line), D2, and the subdomain linker (red line) before RNA binding. Disruption of the interdomain interactions is required for the large-scale conformational changes to the closed state. Destabilization of this Prp5p conformation allows a faster transition from the open state to the active closed state and resulted in enhanced splicing fidelity.

and prior to the BS:U2 duplex formation, resulting in an abortive splicing process (Figure 6B).

In higher eukaryotes, sequences of conserved intron elements, including branch site region, 5′ and 3′ splice sites, are more flexible than in budding yeast (Burge et al., 1999). We analyzed the homologies of primary sequences and secondary structures of Prp5p from yeast, *Drosophila*, and humans and found that residues involved in the interdomain interactions are either conserved at the level of primary sequences or in conserved secondary structures (Figure S2B). It would be interesting to know whether and how this twisted open state conformation of Prp5p exists in higher eukaryotes where the BS region of introns is often more flexible.

EXPERIMENTAL PROCEDURES

Protein Purification

Recombinant *S. cerevisiae* $Prp5p^{206–699}$ was cloned into pSJ2 (a derivative of pET21a) and overexpressed in *E. coli* BL21(DE3) as an N-terminal His_6-tagged protein with induction by 0.2 mM isopropyl-β-D-thiogalactopyraniside when the cell density reached an optical density 600 of 0.6. After growth for overnight at 16°C, the cells were harvested and resuspended in buffer containing 50 mM Tris-HCl (pH 8.0), 500 mM NaCl, 25 mM imidazole, 5 mM β-mercaptoethanol, and 1 mM phenyl-methyl-sulphonyl fluoride, then lysed by French Press. Prp5p was subsequently purified over a nickel affinity column (Chelating Sepharose Fast Flow, GE Healthcare), cleaved by tobacco etch virus protease, and further purified by hydroxyapatite (CHT-I, Bio-Rad) and gel-filtration chromatography (Superdex-75, GE Healthcare). The peak fraction was collected and concentrated to about 25 mg/ml for crystallization. The selenomethionine-labeled Prp5p (SeMet-Prp5p) was generated using the method as described (Doublié, 1997).

Crystallization and Data Collection

Crystals of Prp5p were grown at 20°C using a hanging-drop vapor-diffusion method. Two conditions yielded diffraction quality crystals: (a) 100 mM 2-(*N*-morpholino)ethanesulfonic acid (pH 6.5), 25% polyethylene glycol 4000 and (b) 100 mM Bis-Tris propane (pH 6.5), 20% polyethylene glycol (PEG) 3350 and 200 mM NaF. Crystals grown in condition a belong to the space group $P4_12_12$ diffracted to 2.56 Å, whereas those in condition b belong to the space group $P2_12_12$ diffracted to 2.05 Å. Crystals of SeMet-Prp5p in complex with ADP were grown at 20°C by a sitting-drop vapor-diffusion method by mixing the SeMet-labeled protein (12 mg/ml), 2 mM ATP, and 10 mM $MgCl_2$ with an equal volume of reservoir solution containing 100 mM HEPES (pH 8.0), 21% PEG3000, and 200 mM sodium acetate. Prior to data collection, apo-Prp5p and the complex crystals were equilibrated in a cryoprotectant buffer containing the well solution plus 20% glycerol (or 15% 2-methyl-2,4-pentanediol) and were flash-frozen in liquid nitrogen. All data sets were collected at a BL17U1 beam-line at Shanghai Synchrotron Radiation Facility. All the diffraction data were integrated and scaled using the HKL2000 package (Otwinowski and Minor, 1997).

Structure Determination

Structure of SeMet-Prp5p in complex with ADP was determined by SAD. Thirteen selenium sites were found with SHELX C/D/E (Schneider and Sheldrick, 2002), giving an overall figure of merit of 0.474 as calculated by PHENIX (Adams et al., 2002). The atomic model was built using ARP/wARP (Perrakis et al., 1999) and COOT (Emsley and Cowtan, 2004) and refined with PHENIX. Structures of apo-Prp5p were determined by molecular replacement using Phaser (McCoy et al., 2007) and the atomic coordinates of SeMet-Prp5p-ADP complex as the search model. Iterative cycles of model rebuilding and refinement were carried out using COOT, Refmac5 (Murshudov et al., 1997), and PHENIX. TLS refinement was applied to improve the electron density map (Painter and Merritt, 2006). The refinement statistics are summarized in Table 1. The subdomains D1 and D2 of Prp5p were superimposed with those of Mss116p using Lsqkab in CCP4 suite (Collaborative Computational Project, Number 4, 1994).

Yeast Strains and Copper Assay

S. cerevisiae strains used in this study were derived from yYZX02 (*MATa, ade2 cup1Δ::ura3 his3 leu2 lys2 prp5Δ::loxP trp1*, pRS316-PRP5[*PRP5 URA3* CEN ARS]). Copper assays were carried out as described (Lesser and Guthrie, 1993; Xu and Query, 2007). Plates were scored by the maximum copper concentrations of strain growth and photographed after 4 days at 30°C. For simplicity, growth of each strain with a reporter on three representative copper concentrations was chosen to illustrate altered splicing activities by *prp5* alleles.

In Vitro ATP Hydrolysis Assay

Full-length His6-tagged WT and mutant Prp5p proteins used in ATP hydrolysis assays were expressed in *E. coli*, purified by Ni-NTA agarose (QIAGEN), and

dialyzed into buffer D (20 mM HEPES-KOH [pH 7.9], 0.2 mM EDTA, 100 mM KCl, 0.5 mM dithiothreitol, 1 mM phenylmethylsulfonyl fluoride, and 20% glycerol). ATP hydrolysis assays were performed as described (Tanaka and Schwer, 2006) with modifications. The reaction was first incubated at 30°C for 2 min in 10 μl containing 45 mM Tris-HCl (pH 8.0), 2.2 mM dithiothreitol, 25 mM NaCl, 100 μM EDTA, 1 mM ATP-Mg^{2+}, 0.01% Triton X-100, 50 nM proteins, and poly(A) RNA substrate (Sigma) and then quenched by adding 100 μl of Biomol Green (Enzo Life Sciences) for phosphate detection according to the manual. Values of $K_{m(RNA)}$ and k_{cat} were determined by Lineweaver-Burk plots using GraphPad Prism 5; all values were averages from at least two independent measurements.

ACCESSION NUMBERS

The crystal structures of Prp5p-Mg^{2+}ADP and apo-Prp5p have been deposited in the Protein Data Bank under ID codes 4LJY and 4LK2, respectively.

SUPPLEMENTAL INFORMATION

Supplemental information includes four figures can be found with this article online at http://dx.doi.org/10.1016/j.celrep.2013.10.047.

ACKNOWLEDGMENTS

We thank Charles Query (Albert Einstein College of Medicine) and Zong-Xiang Xia (Shanghai Institute of Organic Chemistry, Chinese Academy of Sciences) for discussions and critical reading of the manuscript. This work was supported by grants from National Basic Research Program of China (2012CB114101 to Y.-Z.X. and 2011CB96630 and 2009CB9186004 to J.Z.), National Natural Science Foundation of China (31270842, 11079051, and 31000340), and the National Grand Project for Medicine Innovation (2011ZX09506-001 to J.Z.).

Received: July 21, 2013
Revised: September 30, 2013
Accepted: October 29, 2013
Published: November 27, 2013

REFERENCES

Adams, P.D., Grosse-Kunstleve, R.W., Hung, L.W., Ioerger, T.R., McCoy, A.J., Moriarty, N.W., Read, R.J., Sacchettini, J.C., Sauter, N.K., and Terwilliger, T.C. (2002). PHENIX: building new software for automated crystallographic structure determination. Acta Crystallogr. D Biol. Crystallogr. *58*, 1948–1954.

Banroques, J., Cordin, O., Doère, M., Linder, P., and Tanner, N.K. (2011). Analyses of the functional regions of DEAD-box RNA "helicases" with deletion and chimera constructs tested in vivo and in vitro. J. Mol. Biol. *413*, 451–472.

Berchtold, H., Reshetnikova, L., Reiser, C.O., Schirmer, N.K., Sprinzl, M., and Hilgenfeld, R. (1993). Crystal structure of active elongation factor Tu reveals major domain rearrangements. Nature *365*, 126–132.

Bleichert, F., and Baserga, S.J. (2007). The long unwinding road of RNA helicases. Mol. Cell *27*, 339–352.

Bono, F., Ebert, J., Lorentzen, E., and Conti, E. (2006). The crystal structure of the exon junction complex reveals how it maintains a stable grip on mRNA. Cell *126*, 713–725.

Burge, C.B., Tuschl, T., and Sharp, P.A. (1999). Splicing of precursors to mRNAs by the spliceosomes. In The RNA World, Second Edition, R.F. Gesteland, T.R. Cech, and J.F. Atkins, eds. (Cold Spring Harbor: Cold Spring Harbor Laboratory Press), pp. 525–560.

Caruthers, J.M., Johnson, E.R., and McKay, D.B. (2000). Crystal structure of yeast initiation factor 4A, a DEAD-box RNA helicase. Proc. Natl. Acad. Sci. USA *97*, 13080–13085.

Collaborative Computational Project, Number 4 (1994). The CCP4 suite: programs for protein crystallography. Acta Crystallogr. D Biol. Crystallogr. *50*, 760–763.

Dalbadie-McFarland, G., and Abelson, J. (1990). PRP5: a helicase-like protein required for mRNA splicing in yeast. Proc. Natl. Acad. Sci. USA *87*, 4236–4240.

Del Campo, M., and Lambowitz, A.M. (2009). Structure of the Yeast DEAD box protein Mss116p reveals two wedges that crimp RNA. Mol. Cell *35*, 598–609.

Doublié, S. (1997). Preparation of selenomethionyl proteins for phase determination. Methods Enzymol. *276*, 523–530.

Emsley, P., and Cowtan, K. (2004). Coot: model-building tools for molecular graphics. Acta Crystallogr. D Biol. Crystallogr. *60*, 2126–2132.

Hahn, D., Kudla, G., Tollervey, D., and Beggs, J.D. (2012). Brr2p-mediated conformational rearrangements in the spliceosome during activation and substrate repositioning. Genes Dev. *26*, 2408–2421.

Högbom, M., Collins, R., van den Berg, S., Jenvert, R.M., Karlberg, T., Kotenyova, T., Flores, A., Karlsson Hedestam, G.B., and Schiavone, L.H. (2007). Crystal structure of conserved domains 1 and 2 of the human DEAD-box helicase DDX3X in complex with the mononucleotide AMP. J. Mol. Biol. *372*, 150–159.

Jankowsky, E., and Fairman, M.E. (2007). RNA helicases—one fold for many functions. Curr. Opin. Struct. Biol. *17*, 316–324.

Kjeldgaard, M., Nissen, P., Thirup, S., and Nyborg, J. (1993). The crystal structure of elongation factor EF-Tu from Thermus aquaticus in the GTP conformation. Structure *1*, 35–50.

Konarska, M.M., Vilardell, J., and Query, C.C. (2006). Repositioning of the reaction intermediate within the catalytic center of the spliceosome. Mol. Cell *21*, 543–553.

Koodathingal, P., Novak, T., Piccirilli, J.A., and Staley, J.P. (2010). The DEAH box ATPases Prp16 and Prp43 cooperate to proofread 5′ splice site cleavage during pre-mRNA splicing. Mol. Cell *39*, 385–395.

Lesser, C.F., and Guthrie, C. (1993). Mutational analysis of pre-mRNA splicing in Saccharomyces cerevisiae using a sensitive new reporter gene, CUP1. Genetics *133*, 851–863.

Linder, P. (2006). Dead-box proteins: a family affair—active and passive players in RNP-remodeling. Nucleic Acids Res. *34*, 4168–4180.

Linder, P., and Jankowsky, E. (2011). From unwinding to clamping - the DEAD box RNA helicase family. Nat. Rev. Mol. Cell Biol. *12*, 505–516.

Maeder, C., Kutach, A.K., and Guthrie, C. (2009). ATP-dependent unwinding of U4/U6 snRNAs by the Brr2 helicase requires the C terminus of Prp8. Nat. Struct. Mol. Biol. *16*, 42–48.

Mallam, A.L., Jarmoskaite, I., Tijerina, P., Del Campo, M., Seifert, S., Guo, L., Russell, R., and Lambowitz, A.M. (2011). Solution structures of DEAD-box RNA chaperones reveal conformational changes and nucleic acid tethering by a basic tail. Proc. Natl. Acad. Sci. USA *108*, 12254–12259.

Mallam, A.L., Del Campo, M., Gilman, B., Sidote, D.J., and Lambowitz, A.M. (2012). Structural basis for RNA-duplex recognition and unwinding by the DEAD-box helicase Mss116p. Nature *490*, 121–125.

Mayas, R.M., Maita, H., and Staley, J.P. (2006). Exon ligation is proofread by the DExD/H-box ATPase Prp22p. Nat. Struct. Mol. Biol. *13*, 482–490.

McCoy, A.J., Grosse-Kunstleve, R.W., Adams, P.D., Winn, M.D., Storoni, L.C., and Read, R.J. (2007). Phaser crystallographic software. J. Appl. Cryst. *40*, 658–674.

Mozaffari-Jovin, S., Santos, K.F., Hsiao, H.H., Will, C.L., Urlaub, H., Wahl, M.C., and Lührmann, R. (2012). The Prp8 RNase H-like domain inhibits Brr2-mediated U4/U6 snRNA unwinding by blocking Brr2 loading onto the U4 snRNA. Genes Dev. *26*, 2422–2434.

Mozaffari-Jovin, S., Wandersleben, T., Santos, K.F., Will, C.L., Lührmann, R., and Wahl, M.C. (2013). Inhibition of RNA helicase Brr2 by the C-terminal tail of the spliceosomal protein Prp8. Science *341*, 80–84.

Murshudov, G.N., Vagin, A.A., and Dodson, E.J. (1997). Refinement of macromolecular structures by the maximum-likelihood method. Acta Crystallogr. D Biol. Crystallogr. *53*, 240–255.

Nguyen, T.H., Li, J., Galej, W.P., Oshikane, H., Newman, A.J., and Nagai, K. (2013). Structural basis of Brr2-Prp8 interactions and implications for U5 snRNP biogenesis and the spliceosome active site. Structure *21*, 910–919.

Otwinowski, Z., and Minor, W. (1997). Processing of X-ray diffraction data collected in oscillation mode. Methods Enzymol. *276*, 307–326.

Painter, J., and Merritt, E.A. (2006). Optimal description of a protein structure in terms of multiple groups undergoing TLS motion. Acta Crystallogr. D Biol. Crystallogr. *62*, 439–450.

Perrakis, A., Morris, R., and Lamzin, V.S. (1999). Automated protein model building combined with iterative structure refinement. Nat. Struct. Biol. *6*, 458–463.

Perriman, R., and Ares, M., Jr. (2000). ATP can be dispensable for prespliceosome formation in yeast. Genes Dev. *14*, 97–107.

Perriman, R., and Ares, M., Jr. (2010). Invariant U2 snRNA nucleotides form a stem loop to recognize the intron early in splicing. Mol. Cell *38*, 416–427.

Perriman, R., Barta, I., Voeltz, G.K., Abelson, J., and Ares, M., Jr. (2003). ATP requirement for Prp5p function is determined by Cus2p and the structure of U2 small nuclear RNA. Proc. Natl. Acad. Sci. USA *100*, 13857–13862.

Ruby, S.W., Chang, T.H., and Abelson, J. (1993). Four yeast spliceosomal proteins (PRP5, PRP9, PRP11, and PRP21) interact to promote U2 snRNP binding to pre-mRNA. Genes Dev. *7*, 1909–1925.

Schneider, T.R., and Sheldrick, G.M. (2002). Substructure solution with SHELXD. Acta Crystallogr. D Biol. Crystallogr. *58*, 1772–1779.

Semlow, D.R., and Staley, J.P. (2012). Staying on message: ensuring fidelity in pre-mRNA splicing. Trends Biochem. Sci. *37*, 263–273.

Sengoku, T., Nureki, O., Nakamura, A., Kobayashi, S., and Yokoyama, S. (2006). Structural basis for RNA unwinding by the DEAD-box protein Drosophila Vasa. Cell *125*, 287–300.

Shao, W., Kim, H.S., Cao, Y., Xu, Y.Z., and Query, C.C. (2012). A U1-U2 snRNP interaction network during intron definition. Mol. Cell. Biol. *32*, 470–478.

Shi, H., Cordin, O., Minder, C.M., Linder, P., and Xu, R.M. (2004). Crystal structure of the human ATP-dependent splicing and export factor UAP56. Proc. Natl. Acad. Sci. USA *101*, 17628–17633.

Staley, J.P., and Guthrie, C. (1998). Mechanical devices of the spliceosome: motors, clocks, springs, and things. Cell *92*, 315–326.

Staley, J.P., and Guthrie, C. (1999). An RNA switch at the 5′ splice site requires ATP and the DEAD box protein Prp28p. Mol. Cell *3*, 55–64.

Story, R.M., Li, H., and Abelson, J.N. (2001). Crystal structure of a DEAD box protein from the hyperthermophile Methanococcus jannaschii. Proc. Natl. Acad. Sci. USA *98*, 1465–1470.

Strauss, E.J., and Guthrie, C. (1994). PRP28, a 'DEAD-box' protein, is required for the first step of mRNA splicing in vitro. Nucleic Acids Res. *22*, 3187–3193.

Tanaka, N., and Schwer, B. (2006). Mutations in PRP43 that uncouple RNA-dependent NTPase activity and pre-mRNA splicing function. Biochemistry *45*, 6510–6521.

Tanner, N.K., and Linder, P. (2001). DExD/H box RNA helicases: from generic motors to specific dissociation functions. Mol. Cell *8*, 251–262.

Villa, E., Sengupta, J., Trabuco, L.G., LeBarron, J., Baxter, W.T., Shaikh, T.R., Grassucci, R.A., Nissen, P., Ehrenberg, M., Schulten, K., and Frank, J. (2009). Ribosome-induced changes in elongation factor Tu conformation control GTP hydrolysis. Proc. Natl. Acad. Sci. USA *106*, 1063–1068.

Wang, Q., He, J., Lynn, B., and Rymond, B.C. (2005). Interactions of the yeast SF3b splicing factor. Mol. Cell. Biol. *25*, 10745–10754.

Warf, M.B., and Berglund, J.A. (2010). Role of RNA structure in regulating pre-mRNA splicing. Trends Biochem. Sci. *35*, 169–178.

Wells, S.E., and Ares, M., Jr. (1994). Interactions between highly conserved U2 small nuclear RNA structures and Prp5p, Prp9p, Prp11p, and Prp21p proteins are required to ensure integrity of the U2 small nuclear ribonucleoprotein in Saccharomyces cerevisiae. Mol. Cell. Biol. *14*, 6337–6349.

Wells, S.E., Neville, M., Haynes, M., Wang, J., Igel, H., and Ares, M., Jr. (1996). CUS1, a suppressor of cold-sensitive U2 snRNA mutations, is a novel yeast splicing factor homologous to human SAP 145. Genes Dev. *10*, 220–232.

Will, C.L., and Lührmann, R. (2011). Spliceosome structure and function. Cold Spring Harb. Perspect. Biol. *3*, a003707.

Xu, Y.Z., and Query, C.C. (2007). Competition between the ATPase Prp5 and branch region-U2 snRNA pairing modulates the fidelity of spliceosome assembly. Mol. Cell *28*, 838–849.

Xu, Y.Z., Newnham, C.M., Kameoka, S., Huang, T., Konarska, M.M., and Query, C.C. (2004). Prp5 bridges U1 and U2 snRNPs and enables stable U2 snRNP association with intron RNA. EMBO J. *23*, 376–385.

Yan, D., and Ares, M., Jr. (1996). Invariant U2 RNA sequences bordering the branchpoint recognition region are essential for interaction with yeast SF3a and SF3b subunits. Mol. Cell. Biol. *16*, 818–828.

Yang, F., Wang, X.Y., Zhang, Z.M., Pu, J., Fan, Y.J., Zhou, J., Query, C.C., and Xu, Y.Z. (2013). Splicing proofreading at 5′ splice sites by ATPase Prp28p. Nucleic Acids Res. *41*, 4660–4670.